Available online at www.sciencedirect.com
ScienceDirect
Journal of Nuclear Materials 361 (2007) 313–321
journal of nuclear materials
www.elsevier.com/locate/jnucmat

Parent–martensite interface structure in ferrous systems

X. Ma *, R.C. Pond

Department of Engineering, University of Liverpool, Brownlow Hill, Liverpool L69 3BX, UK

Abstract

Recently, a Topological Model of martensitic transformations has been presented wherein the habit plane is a semi-coherent structure, and the transformation mechanism is shown explicitly to be diffusionless. This approach is used here to model martensitic transformations in ferrous alloys. The habit plane comprises coherent $(1\,1\,1)_\gamma \| (0\,1\,1)_\alpha$ terraces where the coherency strains are accommodated by a network of dislocations, originating in the martensite phase, and disconnections (transformation dislocations). The disconnections can move conservatively across the interface, thereby effecting the transformation. Since the disconnections exhibit step character, the overall habit plane deviates from the terrace plane. A range of network geometries is predicted corresponding to orientation relationships varying from Nishiyama–Wasserman to Kurdjumov–Sachs. This range of solutions includes habit planes close to $\{2\,9\,5\}$, $\{5\,7\,5\}$ and $\{1\,2\,1\}$, in good agreement with experimental observations in various ferrous alloys.

PACS: 61.50.Ks; 81.30.−t; 68.35.−p; 61.72.−y; 68.35.Dv; 68.37.Lp

1. Introduction

Martensitic transformations are important in a wide range of engineering materials [1] and research in this field has a long history. In the 1950s WLR [2] and BM [3] developed a treatment of the crystallography of martensitic transformations and its predictions are in good agreement with experimental observations for several transformations. The theory is phenomenological, often referred to as the 'Phenomenological Theory of Martensite Crystallography' (PTMC), so does not describe the underlying mechanism of transformation at the atomic level. In the case of ferrous alloys, the PTMC has been used successfully for transformations in high carbon steels and FeNi alloys exhibiting habits near $\{2\,9\,5\}$, but is less satisfactory for $\{5\,7\,5\}$ and $\{1\,2\,1\}$ transformations in lath and plate martensites respectively [4]. An alternative approach has been developed recently in terms of interfacial defects [5,6] and is referred to here as the 'Topological Model' (TM). The TM is a description of the structure of the parent–martensite interface and the line-defects therein; the transformation proceeds by movement of transformation dislocations, or disconnections [7] as they are known, across the interface. This defect motion produces the transformation shear and can be shown explicitly to be diffusionless [8]. To date, the TM has been applied successfully to transformations in a TiMo alloy [5], ZrO_2 [9] and PuGa [10]; the

* Corresponding author. Tel.: +44 151 794 4671; fax: +44 151 794 4901.
E-mail address: jeffreym@liv.ac.uk (X. Ma).

0022-3115/$ - see front matter © 2007 Elsevier B.V. All rights reserved.
doi:10.1016/j.jnucmat.2006.12.009

objective of the present work is to report progress with transformations in ferrous alloys. The principles of the TM are set out in the next section, and subsequently applied to ferrous alloys. Finally, experimental observations of transformations in ferrous systems previously reported in the literature are compared with the present modelling.

2. Topological procedures

By way of introduction to the physical principles of the TM it is helpful to recall briefly the basis of the PTMC. Underlying the PTMC is the hypothesis that the habit plane is an invariant plane of the shape transformation [2,3], so that the parent and martensite crystals fit together there without strain. An algorithm for determining this plane, the transformation displacement and the orientation relationship (OR) of the adjacent phases is expressed in terms of homogeneous deformations represented by matrices [11]. Thus, the principal concern in the PTMC is to find a transformation interface that minimises the elastic strain of the system. In the TM, one also seeks a misfit-free habit plane, but explicit confirmation is additionally required that this interface can migrate without concomitant long-range diffusion. This latter requirement imposes severe constraints on dislocation-based mechanisms and hence leads to a practicable method for identifying possible transformation crystallography. Developments in dislocation theory pertaining to these two aspects of the TM, namely (i) glissile motion of disconnections in interphase interfaces and (ii) misfit accommodation in these interfaces, are reviewed briefly below.

The rules governing glide and climb of dislocations in the bulk of single crystals are well known [12]; glissile motion occurs when a dislocation moves in a plane containing its line direction, $\boldsymbol{\xi}$, and Burgers vector, $\mathbf{b}$. Otherwise, climb occurs, requiring a flux of material to diffuse to or away from a defect's core. In the case of interfacial defects, the situation is more complex because these may exhibit step nature, with height h, in addition to dislocation character – defects are characterised by the couple $(\mathbf{b}, h)$. Also, the density and composition of the adjacent crystals may be different. Hirth and Pond [13] showed that the diffusive flux accompanying motion of a unit length of interfacial defect moving unit distance along an interface is determined by two terms. The first term is equal to the product $h\Delta X$, where ΔX represents the differential atomic concentration of a given species in the parent and martensite phases, and the second is $b_z X$, where b_z is the component of $\mathbf{b}$ perpendicular to the interface plane and X is the concentration in one of the crystals [13]. The second term is directly analogous to the single crystal case mentioned above; thus, if the first term is zero, glide and climb of interfacial defects is governed by the same rule as for single crystals. This occurs, for instance, for defects with $h = 0$, such as crystal or twinning dislocations from either the parent or martensite phases. We adopt the nomenclature of the PTMC for such defects, i.e., 'lattice-invariant deformation' (LID). In the case of disconnections, for which h is always finite, glissile motion can only arise where the chemical composition of the two phases is identical and the two terms above are equal and opposite. In other words, glissile disconnection motion must conserve atomic species, but not necessarily atomic volume as in the single crystal case. This latter condition is only fulfilled by disconnections in a restricted class of interphase boundaries, the most important instance being coherent interfaces [8,14]. Thus, a fundamental step in the TM of a transformation is to identify a candidate interface between the phases that exhibits coherency; this is referred to as a terrace plane. Feasible terrace planes in stiff engineering materials are expected to have relatively modest coherency strains. Once a terrace plane has been identified, the set of LID, $(\mathbf{b}, 0)$, and glissile disconnections, $(\mathbf{b}, h)$, that can arise therein can be determined using the theory of interfacial defects [15].

The coherency strains arising at a terrace plane must be relieved by arrays of interfacial defects. An array of appropriately oriented and spaced glissile disconnections can be one of these sets, and synchronous motion of this set can thereby provide the dual function of effecting the transformation and partially relieving the coherency strain. The second set of defects necessary for complete misfit relief need not be glissile in the interface; however, they will intersect the disconnection array, and these intersections must not impede the glissile motion of the former. In other words, the intersections must themselves be glissile [16,17]; it has been shown that, in general, this only arises if the second set is comprised of LID able to reach the interface by gliding through the martensite phase. Thus, the parent–martensite interface is envisaged as coherent terraces reticulated by arrays of disconnections and LID (slip or twinning), as depicted schematically in Fig. 1. Because of the step character of the disconnections, the overall interface plane, or habit

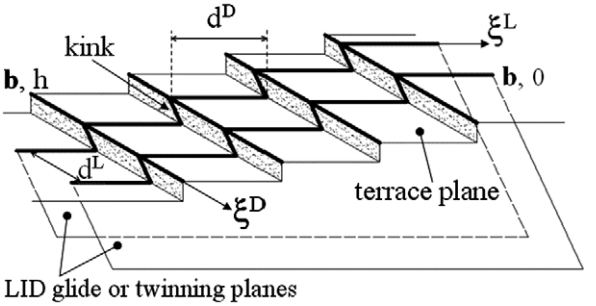

Fig. 1. Schematic illustration of a parent–martensite interface showing the terrace segments and defect arrays. Coherently strained terraces are reticulated by arrays of disconnections $(\mathbf{b},h)$ and crystal slip or twinning dislocations $(\mathbf{b},0)$ from the (lower) martensite crystal.

plane, deviates from the terrace plane. At equilibrium, the spacing of the disconnections, d^{D}, and LID, d^{L}, and their line directions, ξ^{D} and ξ^{L}, must be adjusted until the misfit is fully relieved along the habit plane.

The three stages for determining a misfit-relieved glissile habit plane are summarised schematically in Fig. 2.

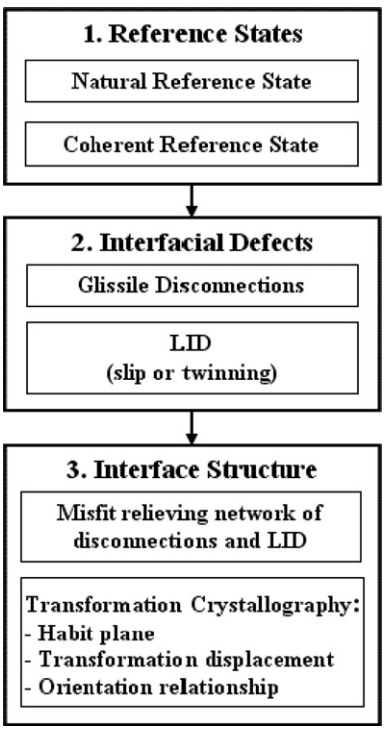

Fig. 2. Schematic summary of the three stages in the topological model for determining a misfit-relieved glissile habit plane, transformation displacement and orientation relationship.

Stage 1: Reference states.

Initially, the two phases are juxtaposed with a chosen OR and exhibiting their natural lattice parameters – the natural reference state. Next, the parent and martensite crystals are strained into coherence on the terrace plane – the coherent reference state; the necessary deformations of the parent and martensite crystals are represented by the matrices ${}_c\mathbf{P}_n$ and ${}_c\mathbf{M}_n$ respectively. The total strain in the terrace plane is then defined by

$$ {}_n\mathbf{E}_c = ({}_c\mathbf{P}_n^{-1} - {}_c\mathbf{M}_n^{-1}). \tag{1}$$

This can be expressed using the terrace plane coordinate frame as

$$ {}_n\mathbf{E}_c = \begin{pmatrix} \varepsilon_{xx} & 0 & 0 \\ 0 & \varepsilon_{yy} & 0 \\ 0 & 0 & 0 \end{pmatrix}, \tag{2}$$

where ε_{xx} and ε_{yy} are the principal strains in the terrace plane. Alternative natural reference states can be chosen where the two crystals are respectively rotated by the angles $\pm\omega/2$ about the normal to the terrace plane, represented by the matrices $\mathbf{R}^{+}$ and $\mathbf{R}^{-}$.

Stage 2: Interfacial defects.

The set of LID and disconnections that can arise in the coherent reference state are determined using the topological theory of interfacial defects [15]. From this set, the subset of disconnections $(\mathbf{b},h)$ that are glissile in the terrace plane can be determined, and also the slip or twinning LID systems that do not form sessile intersections with the disconnections.

Stage 3: Interface structure and transformation crystallography.

The first step in this final stage is to determine the line directions and spacings of the arrays of disconnections and LID that accommodate the coherency strain. These are related to the coherency strains by the Frank–Bilby equation [18]; if the strains defined in Eq. (1) are elastic and are relieved plastically by defect arrays, and any supplementary rotation is also accommodated by defects, we have

$$ \mathbf{B} = (-{}_n\mathbf{E}_c + \mathbf{R})\mathbf{v} = \mathbf{F}\mathbf{v}, \tag{3}$$

where $\mathbf{B}$ is the total Burgers vector crossed by a probe vector $\mathbf{v}$ lying in the interface, and

$$ \mathbf{R} = (\mathbf{R}^{-})^{-1} - (\mathbf{R}^{+})^{-1}. \tag{4}$$

The matrix $(-{}_n\mathbf{E}_c + \mathbf{R})$, designated $\mathbf{F}$, defines the closure failure of a Burgers circuit associated with

the vector **v**. The individual disconnections and dislocations cut by **v** have topological parameters $(\mathbf{b}, h)$ and $(\mathbf{b}, 0)$ defined in the coherent dichromatic pattern. Eq. (3) cannot be solved directly because the habit plane orientation is not known at this stage, and hence **v** cannot be defined. A practicable way forward is to find an approximate solution first and subsequently refine this iteratively. Approximate solutions can be found by neglecting the step character of disconnections, so the interface is imagined to be parallel to the terrace plane; Eq. (3) can then be applied to find a disconnection/LID network accommodating the coherency strain. To refine this solution, the re-oriented interface can be found when the step character of the disconnection array in the approximate solution is taken into account. Then, new probe vectors can be used in Eq. (3), and the defect line directions and spacings modified as required until the misfit on the final habit plane is fully relieved. This procedure has been described in detail elsewhere [6,19] for the cases of a TiMo alloy and ZrO_2. Once a refined solution is obtained, the final OR, which generally deviates from the natural reference OR, can be determined. Also, the transformation displacement, which convolutes the lattice deformation introduced by disconnection motion, the shear introduced by the LID and any deviation of OR from the natural reference, can be found.

3. Interface structure in ferrous alloys

Stage 1: Reference structures.

A convenient choice of natural reference structure for γ-FCC and α-BCC crystals is the Nishyama–Wassermann (NW) OR [20,21], as depicted schematically in Fig. 3. In this OR the closest-packed planes of the two phases are parallel, i.e. $(1\,1\,1)_\gamma \| (0\,1\,1)_\alpha$; these are potential terrace planes and the axes of the terrace coordinate frame are indicated in the figure. The lattice parameters of the cubic crystals used in this work are $a_\gamma = 0.3580$ nm and $a_\alpha = 0.2870$ nm, leading to misfit parallel to x, y and z.

The misfit parallel to x and y is now removed by the coherency strain, thereby forming the coherent reference, and the corresponding dichromatic pattern is depicted in Fig. 4. The strain is given by

$$ {}_n\mathbf{E}_c = \begin{pmatrix} -0.1254 & 0 & 0 \\ 0 & 0.0772 & 0 \\ 0 & 0 & 0 \end{pmatrix}, \qquad (5) $$

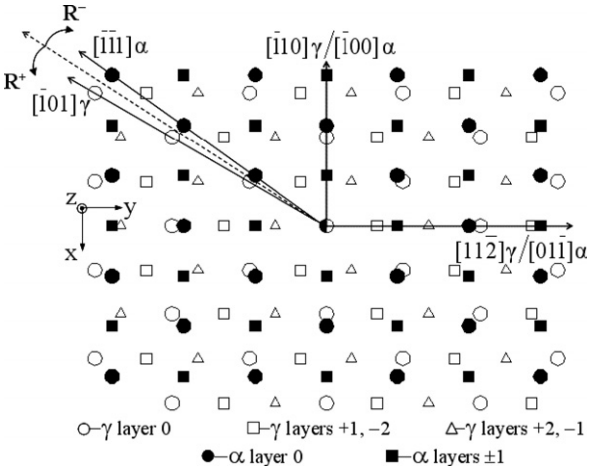

Fig. 3. Schematic illustration showing the natural reference state formed by α and γ crystals exhibiting the NW OR viewed perpendicular to $(1\,1\,1)_\gamma \| (0\,1\,1)_\alpha$; the lattice sites are depicted in white, γ, and black, α, forming a dichromatic pattern.

and we note that the sign of ε_{xx} is negative corresponding to compression of α with respect to γ, whereas ε_{yy} is positive. These principal strains are further depicted in Fig. 5; the rhombi delineating the atomic sites on the $(1\,1\,1)_\gamma \| (0\,1\,1)_\alpha$ planes in the unstrained and coherent states are shown.

Stage 2: Interfacial defects.

The elastic strain defined above is relieved plastically by incorporation into the interface of admissible interfacial defects. Their Burgers vectors and step heights are conveniently illustrated in the coherent dichromatic pattern, Fig. 4. Slip dislocations of the martensite have **b** corresponding to black-to-black translation vectors, **t**(α), for example

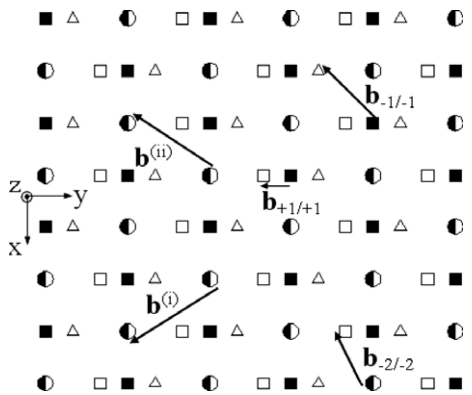

Fig. 4. Schematic illustration of the coherent dichromatic pattern; the **b** of candidate disconnections, joining sites of opposite colour, and LID, joining sites of the same colour, are also shown.

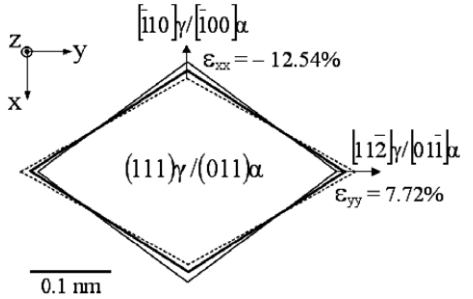

Fig. 5. Scale drawing of the atomic rhombi in the terrace plane of a ferrous alloy. Full lines represent the unstrained martensite, dashed lines the unstrained parent crystal, and bold lines the coherent state.

$\mathbf{b}^{(i)}$ and $\mathbf{b}^{(ii)}$ are derived from $\frac{1}{2}[1\,\bar{1}\,1]_\alpha$ and $\frac{1}{2}[\bar{1}\,\bar{1}\,1]_\alpha$ respectively; these dislocations do not exhibit step character when embedded in the terrace plane. Disconnections have $\mathbf{b}$ corresponding to black-to-white vectors, $\mathbf{t}(\gamma) - \mathbf{t}(\alpha)$, in a dichromatic pattern, and three examples are depicted in Fig. 4 and their parameters are listed in Table 1. One is designated $\mathbf{b}_{-1/-1}$ to indicate that its step goes downwards into the (lower) martensite crystal by one $(1\,1\,1)_\gamma$ and one $(0\,1\,1)_\alpha$ plane, the second has a step twice this height, and the third has a step of opposite sense to the first; the magnitudes of these Burgers vectors relative to $|\mathbf{b}^{(i)}|$ are 0.78, 0.61 and 0.28 respectively. A schematic illustration of $\mathbf{b}_{-1/-1}$, $\mathbf{b}_{-2/-2}$ and $\mathbf{b}_{+1/+1}$ disconnections is shown in Fig. 6; for clarity, the line direction of these defects is taken to be $[\bar{1}\,0\,1]_\gamma/[\bar{1}\,\bar{1}\,1]_\alpha$, so they exhibit mixed character in the figure. These are glissile in the terrace plane despite their components b_z. In the coherent state, the number of atoms per unit area of the $(1\,1\,1)_\gamma$ and $(0\,1\,1)_\alpha$ planes are equal, so motion of disconnections across the terrace plane conserves the number of atoms, but does not conserve volume because the inter-planar spacings of the $(1\,1\,1)_\gamma$ and $(0\,1\,1)_\alpha$ planes are not equal. This glissile motion can be confirmed by using the analysis of Hirth and Pond [13] outlined above. Intersections of $\mathbf{b}_{-1/-1}$ and $\mathbf{b}_{-2/-2}$ disconnections with $\mathbf{b}^{(i)}$ and $\mathbf{b}^{(ii)}$ slip dislocations for example are glissile [17]. Similarly, intersections of $\mathbf{b}_{+1/+1}$ disconnections with twinning dislocations such as $\frac{1}{6}[1\,\bar{1}\,1]_\alpha$ and $\frac{1}{6}[\bar{1}\,\bar{1}\,1]_\alpha$ are glissile.

Stage 3: Misfit relief.

The first step is to find a network comprising one array of LID and a second array of disconnections that accommodates the misfit on the terrace plane. For this 'unrefined' stage, the small components b_z of the disconnections are suppressed temporarily (these produce small ancillary tilts about the defect line, and do not produce long-range displacement fields). Solutions can then be found using the Frank–Bilby equation in expression 3 for the NW OR, or alternative natural reference states with finite values of ω. The spacing of the disconnections, d^D, and LID, d^L, and their line directions, $\boldsymbol{\xi}^D$ and $\boldsymbol{\xi}^L$, are treated as variable quantities in order to find solutions. A practicable procedure is as follows; since two arrays are present it is possible to choose a probe vector $\mathbf{v}^D$ parallel (or anti-parallel) to $\boldsymbol{\xi}^D$ that intersects only LID, and similarly a vector $\mathbf{v}^L$ parallel (or anti-parallel) to $\boldsymbol{\xi}^L$, cutting only disconnections. Thus, in the former case, the Burgers vector cut per unit length, $\mathbf{B}^L$, can be expressed as

$$\mathbf{B}^L = \frac{\mathbf{b}^L \sin(\theta^D - \theta^L)}{d^L} \tag{6a}$$

and in the latter as

$$\mathbf{B}^D = \frac{\mathbf{b}_{p/q} \sin(\theta^D - \theta^L)}{d^D}, \tag{6b}$$

where θ^D and θ^L are the angles subtended by $\boldsymbol{\xi}^D$ and $\boldsymbol{\xi}^L$ from the positive x axis. Eq. (3) can now be expressed as

$$\mathbf{v}^D = \mathbf{F}^{-1}\mathbf{B}^L, \tag{7}$$

and similarly for $\mathbf{v}^L$. Thus, both the directions and magnitudes of $\mathbf{v}^D$ and $\mathbf{v}^L$ can be determined, hence

Table 1
Topological parameters of interfacial defects

	b_x (nm)	b_y (nm)	b_z (nm)	h[a]	$\mathbf{t}(\gamma)$	$\mathbf{t}(\alpha)$
$\mathbf{b}^{(i)}$	0.135	−0.211	0	0	–	$\frac{1}{2}[1\,\bar{1}\,1]_\alpha$
$\mathbf{b}^{(ii)}$	−0.135	−0.211	0	0	–	$\frac{1}{2}[\bar{1}\,\bar{1}\,1]_\alpha$
$\mathbf{b}_{-1/-1}$	−0.135	−0.141	−0.004	−1	$\frac{1}{2}[\bar{1}\,\bar{1}\,0]_\gamma$	$\frac{1}{2}[1\,\bar{1}\,\bar{1}]_\alpha$
$\mathbf{b}_{-2/-2}$	−0.135	−0.070	−0.008	−2	$\frac{1}{2}[\bar{2}\,\bar{1}\,\bar{1}]_\gamma$	$[0\,\bar{1}\,\bar{1}]_\alpha$
$\mathbf{b}_{+1/+1}$	0	0.070	0.004	+1	$\frac{1}{2}[0\,1\,1]_\gamma$	$\frac{1}{2}[\bar{1}\,1\,1]_\alpha$

[a] The 'overlap' step height, h, is defined as the smaller of the terrace plane spacings, i.e. $(0\,1\,1)_\alpha$ in the present case.

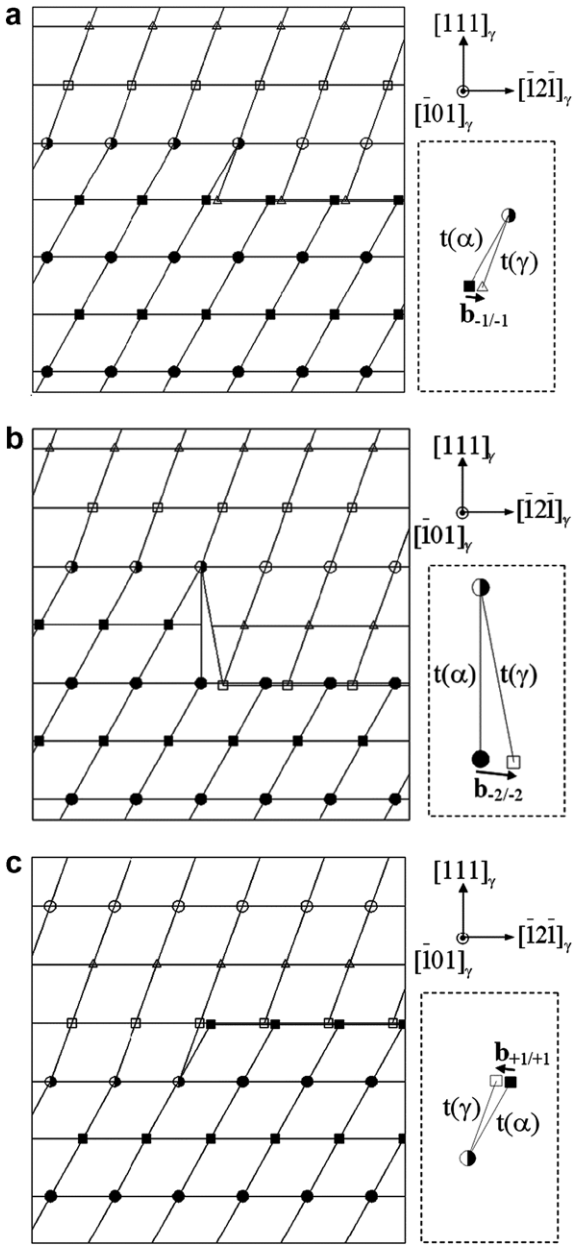

Fig. 6. Schematic illustration of (a) $\mathbf{b}_{-1/-1}$, (b) $\mathbf{b}_{-2/-2}$ and (c) $\mathbf{b}_{+1/+1}$ disconnections in the coherent reference interface viewed along $[\bar{1}\,0\,1]_\gamma/[\bar{1}\,\bar{1}\,1]_\alpha$. Lateral motion of these defects would cause transformation in a conservative manner. The symbols represent site levels along $[1\,1\,1]_\gamma/[0\,1\,1]_\alpha$ as in Fig. 4.

giving the unit vectors $\boldsymbol{\xi}^{\mathrm{D}}$ and $\boldsymbol{\xi}^{\mathrm{L}}$ (from which θ^{D} and θ^{L} are found) and the separations d^D and d^{L}. Network parameters, θ^{L}, d^{L}, θ^{D} and d^{D} for the range of ORs from NW to the KS variant where $[\bar{1}\,0\,1]_\gamma$ is parallel to $[\bar{1}\,\bar{1}\,1]_\alpha$[22], i.e. $\omega = 0°$ to 5.26°, are listed in Table 2 for $\mathbf{b}^{(\mathrm{i})}$ and $\mathbf{b}_{-1/-1}$ defects,

Table 2
Network parameters for $\mathbf{b}^{(\mathrm{i})}$ LID and $\mathbf{b}_{-1/-1}$ disconnections

ω (°)	θ^{L} (°)	d^{L} (nm)	θ^{D} (°)	d^{D} (nm)	ψ (°)
0	59.43	2.319	111.50	1.670	6.93
0.5	60.82	2.520	113.93	1.571	7.36
1.0	62.47	2.757	116.08	1.481	7.80
1.5	64.47	3.039	118.00	1.399	8.26
2.0	66.92	3.381	119.71	1.324	8.72
2.5	69.98	3.801	121.25	1.256	9.18
3.0	73.90	4.320	122.64	1.193	9.65
3.5	79.02	4.969	123.89	1.137	10.12
4.0	85.87	5.775	125.03	1.084	10.60
4.5	95.18	6.736	126.07	1.037	11.08
5.0	107.70	7.745	127.03	0.992	11.56
5.26	115.73	8.200	127.50	0.971	11.81

and a schematic illustration of the network for $\omega = 2.5°$ is shown in Fig. 7(a). The network parameters for $\mathbf{b}^{(\mathrm{i})}$ LID and $\mathbf{b}_{-2/-2}$ disconnections are listed in Table 3 and the network for $\omega = 2.5°$ is depicted in Fig. 7(b). Parameters for the case where the LID is $(1\,1\,2)_\alpha$, $\frac{1}{6}[\bar{1}\,\bar{1}\,1]_\alpha$ twinning are shown in Table 4, and a network corresponding to $\omega = 0.9°$ is depicted in Fig. 7(c). Twinning dislocations are taken to be individually spaced by d^{L} in this figure rather than bunched into twins; the twin fraction corresponding to the same defect density can be readily determined.

The first stage of refinement for the solutions described above is to introduce the step character of the disconnections and hence define the provisional habit plane. The normal to this plane is determined by rotating the normal to the terrace plane by the angle $\psi = \tan^{-1}\frac{h}{d^{\mathrm{D}}}$ about an axis parallel to $\boldsymbol{\xi}^{\mathrm{D}}$ and the values so obtained are included in Tables 2–4. The habit planes for the configurations depicted in Fig. 7, expressed in the parent crystal frame, are $(0.505\ 0.700\ 0.505)_\gamma$, $(0.382\ 0.841\ 0.382)_\gamma$ and $(0.129\ 0.774\ 0.620)_\gamma$ respectively. Further refinement would require the b_z components of the disconnections to be re-instated and the defect content on the habit plane determined using probe vectors in that plane. At equilibrium, the misfit along this plane must be accommodated by the defect network, and further adjustments of defect line directions and separations may be needed. Defect content with resultant component of $\mathbf{B}$ perpendicular to the final habit plane does not affect misfit-relief; it acts as a low-angle tilt boundary thereby introducing an ancillary change in the OR. This refinement procedure for ferrous alloys will be reported fully in a later paper.

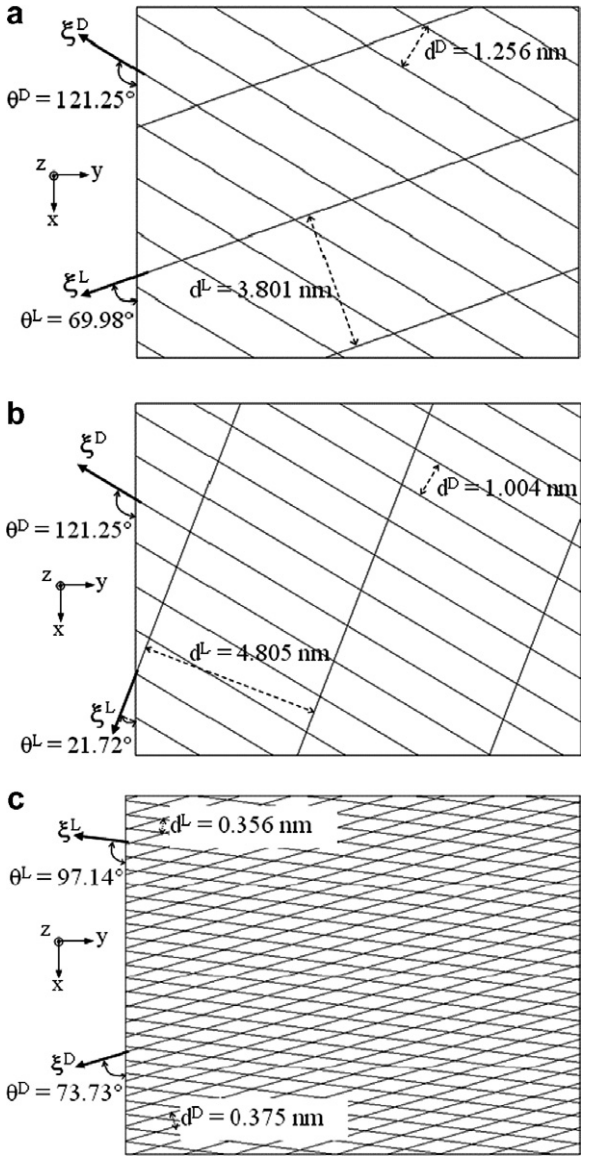

Fig. 7. Schematic illustration of defect networks (a) $\mathbf{b}^{(i)}$ LID and $\mathbf{b}_{-1/-1}$ disconnections for $\omega = 2.5°$, (b) $\mathbf{b}^{(i)}$ LID and $\mathbf{b}_{-2/-2}$ disconnections for $\omega = 2.5°$ and (c) $(1\,1\,2)_\alpha, \frac{1}{6}[\bar{1}\,\bar{1}\,1]_\alpha$ LID and $\mathbf{b}_{+1/+1}$ disconnections for $\omega = 0.9°$.

4. Discussion

The TM of martensitic transformations is based on the principles of dislocation theory, incorporating properly defined reference states and rigorously determined defect content. It provides a physical understanding of processes wherein a misfit-relieved interface can migrate in a diffusionless manner to effect a transformation. Unlike the PTMC, where the interface is a geometrically invariant plane, the TM interface comprises a coherent terrace with an array of LID and disconnections superimposed to relieve misfit. Thus, the TM indicates that the structures of martensitic interfaces are closely related to other semi-coherent interphase interfaces [23,24], but exhibit the special property of glissile disconnections; coherency of the terrace planes is seen to be essential in this context.

The LID and disconnections predicted in the present work are predominantly screw in character, in contrast with misfit-relieving configurations involving edge disconnections, as discussed for example by Rigsbee and Aaronson [25] and Moritani et al. [26]. Thus, the networks predicted here accommodate misfit on the habit plane of martensite in a manner reminiscent of screw dislocation networks in grain boundaries between orthorhombic crystals as discussed by Matthews [27]. Similarly to the grain boundary case, superimposing an additional twist misorientation, ω, has the effect of increasing the spacing of one set of defects in the

Table 3
Network parameters for $\mathbf{b}^{(i)}$ LID and $\mathbf{b}_{-2/-2}$ disconnections

ω (°)	θ^L (°)	d^L (nm)	θ^D (°)	d^D (nm)	ψ (°)
0	40.24	2.784	111.50	1.336	16.89
0.5	37.93	3.057	113.93	1.257	17.90
1.0	35.11	3.382	116.08	1.185	18.91
1.5	31.64	3.772	118.00	1.119	19.94
2.0	27.27	4.242	119.71	1.059	20.97
2.5	21.72	4.805	121.25	1.004	22.22
3.0	14.55	5.463	122.64	0.955	23.03
3.5	5.31	6.185	123.89	0.909	24.06
4.0	−6.33	6.864	125.03	0.868	25.07
4.5	−20.11	7.301	126.07	0.829	26.08
5.0	−34.79	7.305	127.03	0.794	27.08
5.26	−42.30	7.121	127.50	0.776	27.60

Table 4
Network parameters for $(1\,1\,2)_\alpha$, $\frac{1}{6}[\bar{1}\,\bar{1}\,1]_\alpha$ LID and $\mathbf{b}_{+1/+1}$ disconnections

ω (°)	θ^L (°)	d^L (nm)	θ^D (°)	d^D (nm)	ψ (°)
0	90	0.359	68.50	0.334	31.28
0.5	93.98	0.358	71.26	0.356	29.70
0.9	97.14	0.356	73.73	0.375	28.44
1.5	101.80	0.352	77.95	0.405	26.60
2.0	105.56	0.346	82.01	0.433	25.13
2.5	109.14	0.339	86.64	0.461	23.75
3.0	112.67	0.331	91.87	0.490	22.50
3.5	115.99	0.323	97.75	0.517	21.42
4.0	119.12	0.314	104.24	0.541	20.56
4.5	122.08	0.304	111.26	0.559	19.95
5.0	124.86	0.295	118.64	0.569	19.63
5.26	126.26	0.290	122.61	0.570	19.58

network, i.e. either d^{L} or d^{D}, and decreasing the spacing of the other set, as shown in Tables 2–4 and Fig. 7. Therefore, for each of the LID/disconnection combinations chosen here, the TM predicts a range of interface structures consistent with the Frank–Bilby equation and having ORs across the range from NW to KS. In all cases the terrace segments between the defects are coherent, resembling Fig. 4, and the macroscopically determined OR inter-relates the bulk crystals beyond the short-range interfacial displacement field. Optimal structures cannot be identified using geometric criteria alone; energetic and kinetic arguments are needed to resolve this point. A further consideration is that multiple LID modes might operate, as has been proposed by Kelly [28] for example.

Transformation kinetics can also be addressed once a model of the transformation mechanism is established [23]; for the TM, the rate of transformation would be determined primarily by the thermodynamic driving force and the mobility of disconnections. The latter is likely to depend on their screw/edge character, the extent of C-pinning, and the complexity of atomic shuffling accompanying disconnection motion [29].

In our earlier work on TiMo [5], $\boldsymbol{\xi}^{L}$ was taken as being the intersection of the active slip or twinning plane with the habit plane, as depicted in Fig. 1. An important feature of ferrous alloys is that $\frac{1}{2}[1\,\bar{1}\,1]_{\alpha}$ and $\frac{1}{2}[\bar{1}\,\bar{1}\,1]_{\alpha}$ dislocations are glissile in the terrace plane and hence may be able to adjust their line directions after reaching the interface. Thus, in the present work, $\boldsymbol{\xi}^{L}$ is treated as a variable quantity. Of course, for the case of $(1\,1\,2)_{\alpha}$, $\frac{1}{6}[\bar{1}\bar{1}1]_{\alpha}$ twinning in ferrous systems, viable solutions are anticipated to have $\boldsymbol{\xi}^{L}$ close to the intersection of the active twinning plane with the habit plane.

Although the habit plane structures reported here are not fully refined, the provisional structures show good agreement with experimental observations in the literature. For example, Sandvik and Wayman [30] and Kelly et al. [31] studied lath martensite in an FeNiMn alloy using transmission electron microscopy (TEM). They observed an array of $\frac{1}{2}[1\,\bar{1}\,1]_{\alpha}$ LID dislocations with d^{L} in the range 2.6–6.3 nm, $\boldsymbol{\xi}^{L}$ varying between 10° and 15° from screw orientation in a habit plane with $\psi = 9.45°$, and ω ranging between 0.16° and 3.16°. This observation resembles closely the array of $\mathbf{b}^{(i)}$ and $\mathbf{b}_{-1/-1}$ defects predicted here (Table 2 and Fig. 7(a)) for $\omega = 2.5°$, namely: $d^{L} = 3.77$ nm, $\boldsymbol{\xi}^{L}$ oriented 12.99° from screw orientation and habit plane very close to (575). Re-instating the small components of b_z for the $\mathbf{b}^{(i)}$ and $\mathbf{b}_{-1/-1}$ defects produces additional tilts, φ^{L} and φ^{D}, about $\boldsymbol{\xi}^{L}$ and $\boldsymbol{\xi}^{D}$ respectively, where $\varphi^{L} = \sim -0.54°$ and $\varphi^{D} = \sim 0.14°$ in this case; these contributions slightly modify the OR, misaligning the $(1\,1\,1)_{\gamma}$ and $(0\,1\,1)_{\alpha}$ planes for example.

Moritani et al. [26] studied plate martensite in an FeNiMn alloy, and observed an array of $\frac{1}{2}[1\,\bar{1}\,1]_{\alpha}$ LID dislocations with spacing $d^{L} = 4.8$ nm with $\boldsymbol{\xi}^{L}$ close to pure-screw orientation in a habit plane with $\psi = 19.47°$ and $\omega = 1.56°$. This observation resembles the array of $\mathbf{b}^{(i)}$ and $\mathbf{b}_{-2/-2}$ defects predicted in Table 3 for $\omega = 2.5°$, Fig. 7(b), namely: $d^{L} = 4.805$ nm, $\psi = 22°$ and $\boldsymbol{\xi}^{L}$ inclined at 25.39° to screw. The habit plane, for this stage of refinement, $(1, 2.2, 1)_{\gamma}$, is 2.5° from the experimental observation, $(1\,2\,1)_{\gamma}$. In addition, they were able to image the disconnection array using high-resolution TEM. Images obtained with the beam direction parallel $[\bar{1}\,0\,1]_{\gamma}$ closely resemble the defects in Fig. 6(b), bearing in mind the screw component of their Burgers vectors are not evident in such images. Moreover, the average spacing d^{D} observed experimentally is in good agreement with the calculated value of 1 nm for $\mathbf{b}_{-2/-2}$ defects. Mahon et al. [32] and Ogawa and Kajiwara [33] also published images of disconnection arrays in ferrous alloys; these too are consistent with the defects illustrated in Fig. 6(b). In this case $\varphi^{D} = \sim 1.19°$ about $\boldsymbol{\xi}^{D}$ and $\varphi^{L} = \sim -1.01°$ about $\boldsymbol{\xi}^{L}$.

Several researchers have studied ferrous alloys where the martensite plates exhibit habit planes with orientations near $\{2\,9\,5\}_{\gamma}$ or $\{3\,15\,10\}_{\gamma}$ [1,4,11]. The substructures of these plates show internal twinning on $(1\,1\,2)_{\alpha}$, $\langle 1\,1\,1\rangle_{\alpha}$. Using this LID mode, one of the range of TM solutions listed in Table 4, i.e. that with $\omega = 0.9°$, Fig. 7(c), is in reasonable agreement with the experimental data. A more detailed comparison will be made once the TM structure has been refined further.

5. Conclusion

Martensite in ferrous systems has been modelled using the topological method; the interface is semi-coherent and its migration, by lateral motion of disconnections, is conservative and effects the transformation. Dislocation theory has been applied rigorously to find feasible interface structures, although further refinement is needed to establish the equilibrium forms. A variety of LID and discon-

nections is viable in ferrous systems, giving rise to a range of possible transformation crystallographies, including solutions consistent with '(2 9 5)', '(5 7 5)' and '(1 2 1)' habit planes.

Acknowledgement

The authors are grateful to Professors J.P. Hirth and P.M. Kelly for valuable discussion.

References

[1] G.B. Olson, W.S. Owen (Eds.), Martensite, ASM International, USA, 1992.
[2] M.S. Wechsler, D.S. Lieberman, T.A. Read, Trans AIME 197 (1953) 1503.
[3] J.S. Bowles, J.K. MacKenzie, Acta Metall. 2 (1954) 129.
[4] P.G. McDougall, C.M. Wayman, The Crystallography and Morphology of Ferrous Martensites, ASM International, USA, 1992.
[5] R.C. Pond, S. Celotto, J.P. Hirth, Acta Mater. 51 (2003) 5385.
[6] R.C. Pond, X. Ma, Y.W. Chai, J.P. Hirth, in: F.R.N. Nabarro, J.P. Hirth (Eds.), Dislocations in Solids, vol. 13, North-Holland, Amsterdam, 2007.
[7] J.P. Hirth, J. Phys. Chem. Sol. 55 (1994) 985.
[8] R.C. Pond, S. Celotto, Int. Mater. Rev. 48 (2003) 225.
[9] R.C. Pond, X. Ma, J.P. Hirth, Mater. Sci. Eng. A 438–440 (2006) 109.
[10] J.P. Hirth, J.N. Mitchell, D.S. Schwartz, T.E. Mitchell, Acta Mater. 54 (2006) 1917.
[11] C.M. Wayman, Introduction to the Crystallography of Martensite Transformations, Macmillan, New York, 1964.
[12] J.P. Hirth, J. Lothe, Theory of Dislocations, second ed., McGraw-Hill, New York, 1982.
[13] J.P. Hirth, R.C. Pond, Acta Mater. 44 (1996) 4749.
[14] R.C. Pond, X. Ma, Z. Metallkd. 96 (2005) 1124.
[15] R.C. Pond, in: F.R.N. Nabarro (Ed.), Dislocations in Solids, vol. 8, North-Holland, Amsterdam, 1989, p. 1.
[16] J.W. Christian, Metall. Mater. Trans. 25A (1994) 1821.
[17] R.C. Pond, A. Serra, D.J. Bacon, Acta Mater. 47 (1999) 1441.
[18] B.A. Bilby, R. Bullough, E. Smith, Proc. Roy. Soc. 231A (1955) 263.
[19] R.C. Pond, X. Ma, J.P. Hirth, in: J.M. Howe, D.E. Laughlin, J.K. Lee, D.J. Srolovitz, U. Dahmen (Eds.), Solid to Solid Phase Transformations in Inorganic Materials 2005, vol. 2, TMS, Warrendale, 2005, p. 19.
[20] Z. Nishiyama, Sci. Rep. Tohoku Univ. 23 (1934) 637.
[21] G. Wasserman, Mit. Kaiser-Wilhelm Inst. Eisenforsch. 17 (1935) 149.
[22] G.V. Kurdjumov, G. Sachs, Z. Phys. 64 (1930) 325.
[23] A.P. Sutton, R.W. Balluffi, Interfaces in Crystalline Materials, Clarendon, Oxford, 1995.
[24] J.M. Howe, Interfaces in Materials, Wiley, USA, 1997.
[25] J.M. Rigsbee, H.I. Aaronson, Acta Metall. 27 (1979) 365.
[26] T. Moritani, N. Miyajima, T. Furuhara, T. Maki, Scripta Mater. 47 (2002) 193.
[27] J.W. Matthews, Philos. Mag. 29 (1974) 797.
[28] P.M. Kelly, Mater. Trans. JIM 33 (1992) 235.
[29] A.G. Crocker, Philos. Mag. 7 (1962) 1901.
[30] B.P.J. Sandvik, C.M. Wayman, Metall. Trans. 14A (1983) 835.
[31] P.M. Kelly, A. Jostsons, R.G. Blake, Acta Metall. Mater. 38 (1990) 1075.
[32] G.J. Mahon, J.M. Howe, S. Mahajan, Philos. Mag. Lett. 59 (1989) 273.
[33] K. Ogawa, S. Kajiwara, Philos. Mag. 84 (2004) 2919.